fermentation

MDPI

Article

Application of High-Solid Anaerobic Digestion Biogas Residue to Initiate Aerobic Composting of Food Waste: Performance and Mechanisms

Bin Chi [1], Penghui Huang [1], Shenghua Zhang [1,*], Heyong Zhang [1], Jian Wu [1] and Ang Li [2]

[1] College of Harbour and Coastal Engineering, Jimei University, Xiamen 361021, China; binchi@jmu.edu.cn (B.C.); penghuihuang@jmu.edu.cn (P.H.); heyongzhang@jmu.edu.cn (H.Z.); jwu@jmu.edu.cn (J.W.)

[2] State Key Laboratory of Urban-Rural Water Resource and Environment, School of Environment, Harbin Institute of Technology, Harbin 150090, China; li.ang@hit.edu.cn

* Correspondence: shzhang@jmu.edu.cn

Abstract

Aerobic composting of food waste (FW) is constrained by delayed temperature increase initially. This study evaluated the use of high-solid anaerobic digestion (HSAD) biogas residue as a composting initiator. In the co-composting treatment containing biogas residue and FW (C3), the temperature peaked at 69.8 °C on day 5. In comparison, the FW composting alone (C1) reached a lower peak temperature of 67.1 °C on day 8. Similarly, C3 sustained the thermophilic phase (>55 °C) for 10 days, comparable to the 11 days observed in C1. The incorporation of biogas residue adjusted the pH of FW toward neutrality, helping to reduce nitrogen loss. C3 also demonstrated a distinctive phytohormone profile, with salicylic acid (SA) content reaching 42.62 ng g^{-1}, significantly exceeding that of C1 (31.54 ng g^{-1}), suggesting enhanced bio-stimulatory potential. Compared with C1, N_2O emissions in C3 were both reduced and delayed, while cumulative CH_4 emissions were lower than those in the biogas-residue-alone composting (C2). Biogas residue addition introduced thermotolerant microbes, reduced acidification by suppressing acidophiles, and enhanced humification via cooperative networks. Metagenomics revealed that C3 developed a denitrification gene profile favoring net N_2O consumption under high pH. These results demonstrate that HSAD biogas residue can serve as an effective initiator for FW composting.

Keywords: high-solid anaerobic digestion (HSAD); biogas residue; food waste; aerobic composting; initiator

Academic Editor: Giulia Bozzano

Received: 6 June 2026
Revised: 7 July 2026
Accepted: 10 July 2026
Published: 14 July 2026

1. Introduction

Food waste (FW) is a highly biodegradable organic solid waste, and increasing attention has been directed toward its safe disposal and resource utilization. Among the available treatment technologies, aerobic composting is widely recognized as an effective biological approach for FW management. However, composting FW alone is often limited by a slow rate of temperature increase during the initial stage due to its high moisture content, low porosity, and elevated lignocellulosic content [1]. In addition to conventional optimization strategies, such as adjusting moisture content, adding bulking agents, and regulating the carbon-to-nitrogen (C/N) ratio [2,3], more effective approaches are needed to trigger the heating phase of FW composting rapidly. Existing initiation strategies primarily

involve pretreating the composting substrate or adding specific initiators. For example, the introduction of a 24-h pre-biodrying stage combined with enhanced aeration enabled efficient maturation of FW within 10 days [4]. Similarly, sequential inoculation with *Pseudomonas aeruginosa* DO1 and a thermophilic microbial consortium during composting of lipid-rich FW resulted in 91.91% lipid degradation via β-oxidation and a 92.74% increase in humic substance formation [5].

Anaerobic digestion is another important biological technology for FW treatment. Based on the total solids content of the feedstock, anaerobic digestion systems are generally classified as wet (<10% total solids), semi-dry (10–15% total solids), or dry (≥15% total solids) digestion [6]. Dry anaerobic digestion, also known as high-solid anaerobic digestion (HSAD), produces biogas slurry and biogas residue as by-products. Current studies on biogas residue mainly focus on its physicochemical properties, including high carbon content, porous structure, and abundance of stable inorganic constituents, which support its conversion into biochar for further applications. For example, biochar derived from biogas residue has been reported to enhance coenzyme F420 activity in HSAD reactors, thus improving methane production [7]. It has also been applied in electrochemical systems to reduce total nitrogen (TN) and chemical oxygen demand (COD) in aquaculture wastewater [8]. Further, biogas residue has demonstrated potential for removing contaminants such as antibiotics (e.g., ciprofloxacin) [9] and pesticides (e.g., atrazine) [10]. However, the high solids content of HSAD feedstocks often impairs homogenization of the substrate within the reactor, leading to incomplete degradation of organic matter [11]. As a result, HSAD biogas residue typically shows elevated pH, rich microbial diversity, and a high solid content, dominated by cellulose and hemicellulose [12,13], along with readily degradable organic compounds, such as volatile fatty acids, that were not fully converted into methane [14,15].

Considering both the limitations of sole aerobic composting of FW and the distinctive characteristics of HSAD biogas residue, HSAD biogas residue has strong potential to serve as an initiator for FW aerobic composting. Therefore, in this study the specific objectives were: (1) to evaluate the initiating effects of HSAD biogas residue on FW composting and greenhouse gas (GHG) emission characteristics, and (2) to elucidate the mechanisms underlying accelerated compost maturation with physicochemical indicators, 16S rRNA sequencing and metagenomic analyses. This work provides a scientific foundation for developing an efficient and low-GHG-emission composting strategy for FW treatment.

2. Materials and Methods

2.1. Composting Materials and Experiments

The FW and biogas residue were used as the composting substrates. FW was collected from the Caitu Canteen of Jimei University (Xiamen, China), while biogas residue was obtained from the Houkeng Garbage Classification Plant (Xiamen, China). The collected FW was crushed into a paste with a blender before being used in the experiments. The biogas residue was freshly obtained from a high-solid anaerobic digestion (HSAD) system. Briefly, fresh biogas residue samples were randomly collected from the HSAD tank, after which non-biodegradable impurities, including coarse fibers, metals, plastics, and bones, were manually removed. The sorted residue was subsequently ground using a Chinese herbal medicine grinder for further use. In the FW, the protein, lipid, and cellulose contents were 0.88 mg g^{-1}, 12.14%, and 105.53 mg g^{-1} dry weight, respectively, whereas the corresponding values in the biogas residue were 0.37 mg g^{-1}, 3.87%, and 50.18 mg g^{-1} dry weight.

The composting process consisted of a 28-day primary composting stage followed by a 64-day curing stage [16,17]. The primary composting mixtures were prepared in cuboid reactors measuring 38 cm × 18 cm × 25 cm, which were maintained at 37 °C [18].

Three treatment groups were established: C1 (FW composting alone), C2 (biogas residue composting alone), and C3 (equal amounts of biogas residue and FW composting). Here, C1 served as a control for FW-only composting to reveal its inherent heating limitations, C2 as a control for biogas residue-only composting to characterize its rapid heating but short thermophilic phase, and C3 as the initiation treatment to evaluate the initiation effect. In C3, the mixing ratio was determined on a fresh wet-weight basis. To ensure that the initiating effect of biogas residue could be unequivocally observed and to avoid inconclusive results due to insufficient amendment dosage, a 1:1 mixing ratio of biogas residue to FW was adopted in C3 as an initial exploratory strategy. Dry rice husk was added to all treatments to adjust the initial moisture content to 50% [19]. Each composting pile had an initial mass of 8 kg. During the curing composting, the material was placed in static bins (66 cm × 48.6 cm × 40 cm) at room temperature. The composting piles were manually turned thoroughly daily to ensure adequate oxygenation in the pile.

Compost samples were collected daily to determine temperature (T), pH, electrical conductivity (EC), moisture content, and organic matter (OM), and water was added as needed to maintain the moisture content at 50%. Samples collected on days 1, 3, 5, 7, 15, and 28 were further analyzed for total carbon (TC), TN, and C/N ratio. For three-dimensional excitation-emission matrix analysis, samples were obtained during the initial, warming, thermophilic, cooling, and maturation stages, corresponding to days 1, 3, 7, 15, and 23 for C1 and C3, and days 1, 2, 3, 9, and 23 for C2. To investigate the initiation mechanism of biogas residue on aerobic composting of FW, the composting materials of three groups on day 1 were also analyzed as initial materials for dehydrogenase activity (DHA), Ecoplate average well color development (AWCD), protein, lipids, cellulose, volatile fatty acids, COD, and the BOD_5/COD ratio. Samples collected on days 1, 3, 5, 7, and 23, and 92 were subjected to 16S rRNA sequencing, whereas metagenomic analysis was performed using samples collected only on day 7. Samples collected on day 92 were further analyzed for phytohormones, germination index, phosphorus (P), potassium (K), and heavy metals (Cr, As, Cd, Hg, Pb).

Gas samples were collected daily during the first 16 days to monitor emissions of the major GHGs, including carbon dioxide (CO_2), nitrous oxide (N_2O), and methane (CH_4). Sampling was conducted each day between 10:00 and 11:00 AM. Gas samples were collected at 0, 10, 20, and 30 min after sealing the chamber using a 50 mL syringe, and then transferred to Labco tubes for subsequent analysis.

2.2. Physicochemical Properties of Compost Materials and GHGs Analysis

Following the methods described by Chen et al. [19,20], several physicochemical parameters were evaluated, including T, pH, EC, moisture content, OM, TC, TN, C/N ratio, germination index, and the contents of P, K, and heavy metals. The concentration of N_2O was measured using a gas chromatograph (Agilent 7890A, Santa Clara, CA, USA) equipped with an electron capture detector, whereas CO_2 and CH_4 concentrations were analyzed using a gas chromatography system fitted with a flame ionization detector (FID). Gas emission fluxes were calculated according to the method reported by Chen et al. [20].

Protein content was quantified using a Bicinchoninic Acid Protein Assay Kit (B917925, 200T/EA; Macklin Inc., Shanghai, China). Lipid content was determined using a Soxhlet extraction system [21], while cellulose content was measured using a cellulose Content Assay Kit (100T/96S; Jingkelong Biotechnology Co., Ltd., Beijing, China).

Volatile fatty acid concentrations were analyzed according to the method described by Li et al. [21]. DHA was determined using the triphenyl tetrazolium chloride reduction method. Microbial carbon utilization capacity was assessed using EcoPlates, and AWCD was calculated [19]. Three-dimensional excitation-emission matrix fluorescence

spectroscopy was conducted using a fluorescence spectrophotometer (F-390, Tianjin Gangdong Sci.&Tech. Co., Ltd., Tianjin, China) as previously described [22]. The calculation methods for the humification index (HIX) and biological index (BIX) are provided in the Supplementary Materials (Text S1). COD was measured using a COD analyzer (LH-5B3B, Lianhua Technology, Beijing, China), whereas 5-day biochemical oxygen demand (BOD_5) was determined using a BOD analyzer (LH-BOD306, Lianhua Technology, Beijing, China).

2.3. Phytohormones Detection Method

The samples were first homogenized using a high-throughput tissue grinder, and then subjected to ultrasonic extraction and centrifugation. The resulting supernatants were then injected into the LC-MS/MS system for analysis. Detailed experimental procedures are described in the Supplementary Materials (Text S2).

2.4. Microbial Sequencing and Metagenomic Analysis

Microbial DNA was extracted from compost samples using the HiPure Soil DNA Kit (Magen Biotechnology Co., Ltd. Guangzhou, China). The V3–V4 region of the 16S rRNA gene was amplified with universal primers and sequenced on the Illumina NovaSeq platform (Illumina, Inc., San Diego, CA, USA). Raw sequencing data were processed using the DADA2 pipeline to generate amplicon sequence variants, which were subsequently taxonomically classified against the SILVA database. Metagenomic sequencing was carried out on the Illumina NovaSeq X Plus platform. The obtained reads were assembled using MEGAHIT, and gene functional annotation was performed using databases such as Kyoto Encyclopedia of Genes and Genomes. Raw metagenomic sequencing data have been deposited in the National Center for Biotechnology Information Sequence Read Archive under BioProject ID PRJNA1391911. Detailed bioinformatics procedures are described in the Supplementary Materials (Text S3).

2.5. Statistical Analysis

Data visualization was performed using Origin 2021 (OriginLab, Northampton, MA, USA) and GraphPad Prism 10 (GraphPad Software, San Diego, CA, USA). Fluorescence spectrophotometry data were analyzed using MATLAB R2024a (MathWorks, Natick, MA, USA). Relationships between microbial communities and environmental factors were evaluated using Canoco 5.0 (Microcomputer Power, Ithaca, NY, USA). Processing and visualization of microbial sequencing data were conducted through the sequencing service provider's analysis platform. Microbial co-occurrence networks were constructed using Gephi 0.9.7, and network analyses were performed to investigate interactions among microorganisms and environmental variables. Partial least squares path modeling (PLS-PM) was performed in R using the plspm package to elucidate the relationships among different parameters and their contributions to target variables. Detailed information regarding the calculation and interpretation of the manifest variables associated with Composting Heating Performance in the PLS-PM analysis is provided in the Supplementary Materials (Text S4). Data from replicate experiments are presented as mean ± standard deviation. Statistical significance among variables was determined using one-way analysis of variance (ANOVA) in SPSS 22.0, with $p < 0.05$ considered significant.

3. Results and Discussion

3.1. Physicochemical Parameters During Composting

Among the three treatments, C1 showed the slowest rate of temperature increase, reaching a peak of 67.1 °C on day 8. In comparison, C2 showed the fastest heating rate, with a peak temperature of 69.7 °C on day 3. The maximum temperature in C3 reached

69.8 °C on day 5 (Figure 1a). The thermophilic phase (>55 °C) lasted for 11, 5, and 10 days in C1, C2, and C3, respectively. Therefore, all composting treatments satisfied the Chinese composting standard (CJJ 52-2014), which requires temperatures to remain at or above 55 °C for at least five consecutive days. C1 showed a relatively slow heating rate but a prolonged thermophilic phase, whereas C2 displayed rapid heating and a shorter thermophilic phase. In C3, the addition of biogas residue significantly improved the heating rate of FW composting while maintaining a thermophilic duration comparable to that of C1. These results suggest that biogas residue can effectively serve as an initiator to accelerate FW composting.

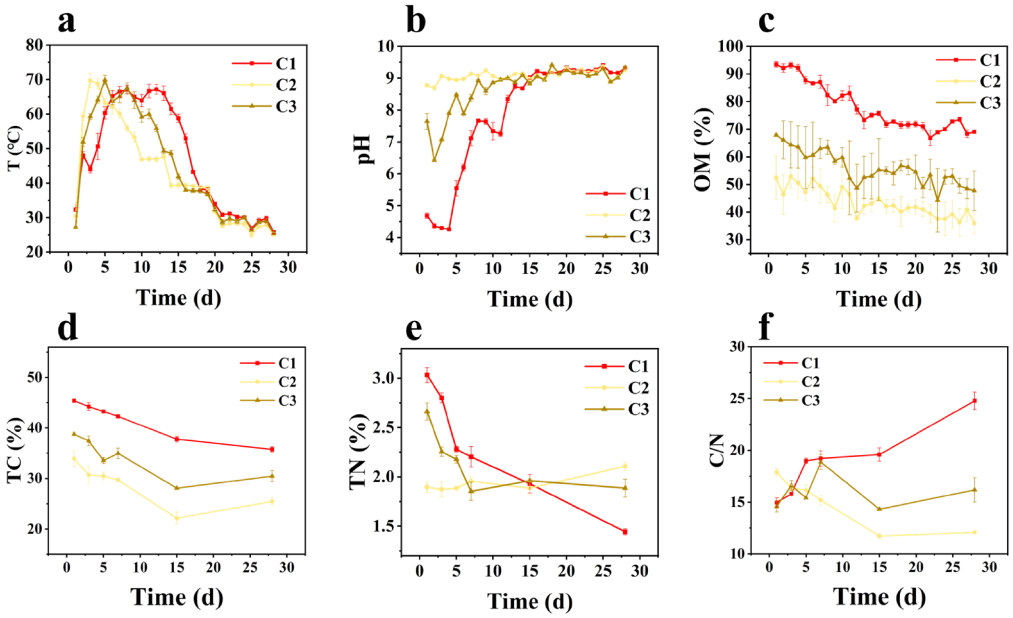

Figure 1. Physicochemical parameters of different treatment groups during composting: (**a**) temperature (T); (**b**) pH; (**c**) organic matter (OM); (**d**) total carbon (TC); (**e**) total nitrogen (TN); and (**f**) carbon-to-nitrogen (C/N) ratio. Values are mean ± SD of five replicates for temperature and of three for other parameters.

Throughout composting, the moisture content in all treatments remained within the range of 44.5–59.9% (Figure S1a), meeting the composting standards [19]. The initial pH values of C1, C2, and C3 were 4.68, 8.78, and 7.64, respectively (Figure 1b). As composting progressed, microbial degradation of nitrogen-containing organic matter generated ammonia, resulting in gradual increases in pH to 9.32, 9.26, and 9.34 in C1, C2, and C3, respectively. In C3, the addition of biogas residue increased the FW pile's initial pH, therefore facilitating compost initiation. By the end of the composting process, the EC values in all treatments were below 3 mS cm^{-1} (Figure S1b), indicating that all compost products had reached a stable state [23].

OM content decreased rapidly during the initial composting stage in all treatments, followed by a gradual decline in the degradation rate, reflecting intensive microbial mineralization of OM (Figure 1c) [19]. According to the Chinese standard for organic fertilizers (NY 525-2021), OM content in organic fertilizer products should exceed 30% on a dry-weight basis. All compost products in this study met this requirement. Previous studies have shown that composting beds containing agroindustrial solid waste from the Amazon region and inoculated with native microorganisms achieved maturity approximately five weeks earlier than uninoculated controls [24]. Similarly, the addition of OM-rich soybean residues has been reported to enhance OM degradation and humification during swine manure composting [25]. In this study, the relative OM reduction rate in C2 was higher

than that observed in C1 and C3 (all $p < 0.05$) (Text S5), likely because microorganisms present in the biogas residue promoted the degradation of readily biodegradable OM. The OM degradation rate in C3 was higher than that in C1, although the difference was not statistically significant ($p > 0.05$). This enhancement was likely attributable to the abundant microorganisms and degradable OM introduced by the biogas residue, which facilitated the initiation of FW composting.

At the end of composting, C2 showed the highest TC removal rate ($p < 0.01$) (Figure 1d). This result may be attributed to the substantial amount of readily degradable OM remaining in the biogas residue that had not been converted into CH_4 during HSAD. On day 28, the greatest TN loss was observed in C1 ($p < 0.001$) (Figure 1e), suggesting that the high nitrogen content of FW, mainly derived from proteins, underwent rapid degradation at a rate exceeding nitrification capacity. Therefore, a considerable amount of nitrogen was lost through ammonia volatilization. Previous studies have similarly reported nitrogen loss rates exceeding 40% during FW composting, particularly under low-C/N-ratio conditions [26], which is consistent with the findings of this study (Figure 1f). In comparison, C2 showed no significant change in TN content ($p > 0.05$). Moreover, the TN loss rate in C3 was lower than that in C1, likely because the biogas residue neutralized the acidic conditions of FW and reduced ammonia volatilization.

3.2. Changes in OM Composition During Composting

Three-dimensional excitation-emission matrix fluorescence spectroscopy was employed to characterize fluorescence spectral indicators associated with compost maturity [27]. On the first day of composting, Region IV, corresponding to soluble microbial by-products, represented the dominant fluorescence fraction in all three treatments (Figure 2a–c). These compounds were mainly derived from microbial activity in the compost piles, where microorganisms promoted the degradation of OM by secreting various hydrolases. As composting progressed, the regional fluorescence integration across all treatments gradually shifted from Regions I, II, and IV toward Region V, indicating a progressive accumulation of fulvic acid-like substances (Figure S2). This observation is consistent with previous studies on sludge-reed co-composting, in which degradation of OM components, including polysaccharides, lipid chains, and proteins, promoted humification as composting advanced [18].

Differences in Region V accumulation further reflected the distinct humification potentials among the three treatments. C1 demonstrated the strongest capacity for humic substance formation, with Region V increasing by 36%. In comparison, C2 showed limited humification potential because of insufficient carbon sources, resulting in only an 18% increase in Region V. The performance of C3 was significantly better than that of C2 and approached the level observed in C1, with a 32% increase in Region V. This result suggested that microorganisms introduced through the biogas residue likely supplied key degradation enzymes to the FW composting system. Therefore, the synergistic interaction between FW and biogas residue promoted humification. From the perspective of OM compositional changes during composting, these results supported the feasibility of using biogas residue as an initiator for FW composting.

The HIX is commonly used to evaluate the degree of humification during composting. In comparison, the BIX reflects the biological origin of dissolved OM and the activity of functional microorganisms [28]. As shown in Figure 2d–f, HIX gradually increased in all treatments throughout composting, indicating continuous accumulation of humic substances. The highest HIX value (0.943) was observed in C1 during the maturation stage (D23), which might be related to the prolonged thermophilic phase in this treatment despite its relatively slow heating rate. This further confirmed the higher humification

degree of C1, consistent with results from fluorescence regional integration analysis. In comparison, C2 showed the highest BIX value (1.788) at the initial stage (D1), suggesting that the biogas residue possessed high biodegradability and rich microbial diversity. By increasing microbial diversity, the addition of biogas residue in C3 appeared to balance humification and microbial metabolic activity, improving overall composting efficiency.

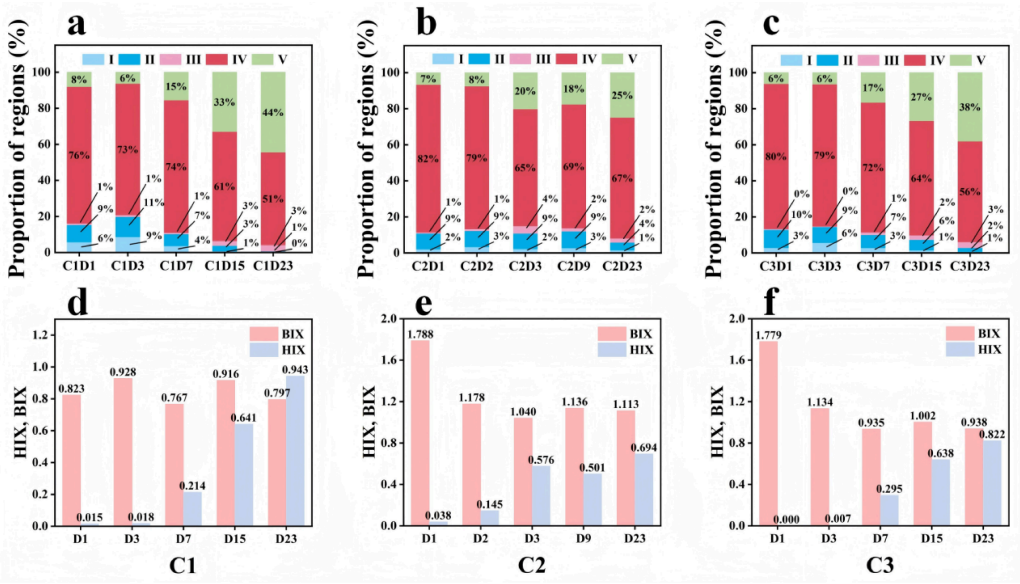

Figure 2. Percentage distributions of fluorescence regional integration (FRI) in five regions (I–V) for the three parallel factor analysis (PARAFAC) components: (**a**) C1, (**b**) C2, and (**c**) C3; values of humification index (HIX) and biological index (BIX) for samples corresponding to (**d**) C1, (**e**) C2, (**f**) C3. The displayed spectra are representative of the triplicate measurements.

3.3. Characteristics of Compost Products

In this study, the concentrations of heavy metals in all three compost products were substantially below the maximum limits specified in the NY/T 525-2021 standard for mature compost (Table S1). The total nutrient content in each treatment met or exceeded the required threshold of 4.0% (Figure 3a).

Phytohormones are known to enhance plant nutrient utilization efficiency and tolerance to abiotic stress [29], while also influencing microbial community structure and metabolic activity during composting [30]. A total of 24 phytohormones were identified and quantified in the compost products (Figure 3c and Table S2). Phytohormones were systematically categorized into nine major classes: gibberellins; auxins; synthetic auxin analogues; conjugated auxins; stress response-related hormones; synthetic cytokinin analogues; cytokinins; abscisic acid; and growth inhibitors/retardants.

3-Indoleacetic acid (IAA), the principal natural auxin in plants, plays a critical role in regulating cell division, elongation, differentiation, and overall plant development [31]. The highest IAA concentration was detected in C1 (13.70 ng g^{-1}), likely because FW contained abundant tryptophan, a key precursor for IAA biosynthesis [32]. Meanwhile, the IAA content in C3 (5.27 ng g^{-1}) was significantly higher than that in C2 (3.99 ng g^{-1}). Several auxin amino acid conjugates, including IAAsp, IAAla, IAPhe, and IATrp, were detected in all treatments, suggesting that the compost products possessed a slow-release IAA reservoir capable of supporting long-term physiological regulation [33]. The moderate level of indole-3-propionic acid (IPA) observed in C3 further reflected the balancing effect of FW co-composting on the auxin profile. Gibberellins (GAs), which are essential for seed germination [34], were also retained at appreciable levels in C3, indicating that co-composting effectively preserved a substantial portion of GAs originating from FW.

Cytokinins, including cZ and iP, were most abundant in C1, and the stress-responsive nature of cZ [35] may have contributed to the compost product's enhanced stress tolerance.

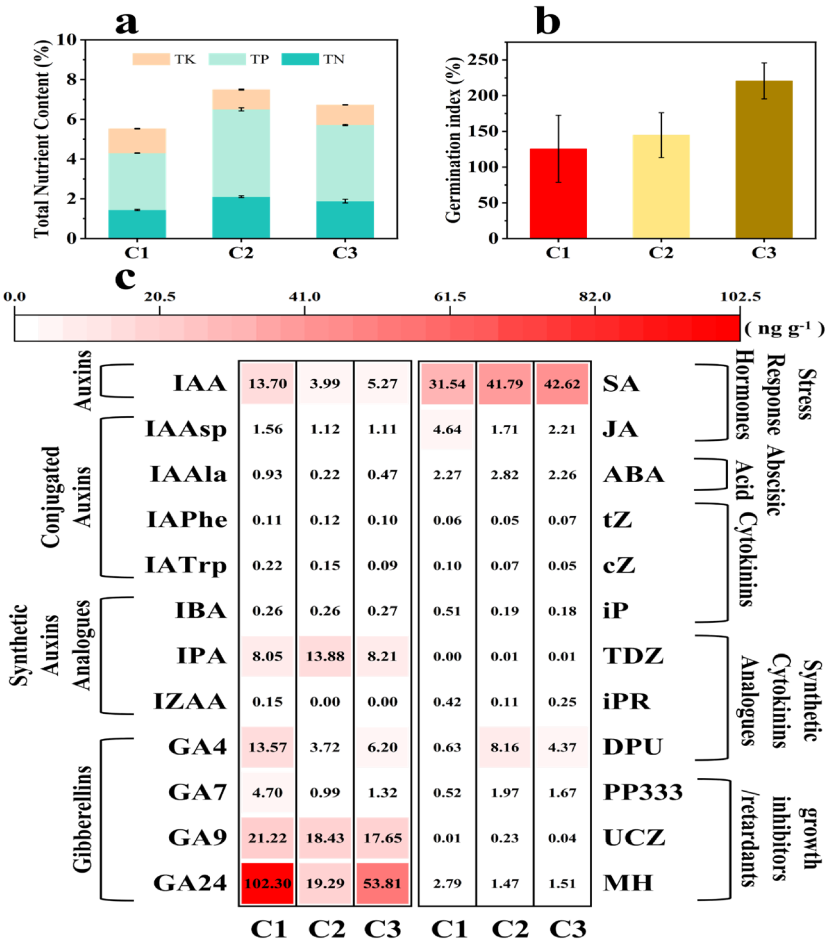

Figure 3. Compost product quality: (**a**) Total nutrient contents, including total potassium (TK), total phosphorus (TP), and TN, (mean ± SD, n = 3); (**b**) Germination index, (mean ± SD, n = 3); (**c**) Concentrations of various phytohormone classes, including gibberellins, auxins and their synthetic analogues and conjugated forms, cytokinins and their synthetic analogues, abscisic acid, stress-related hormones, and growth inhibitors/retardants (n = 3).

Salicylic acid (SA), a key microbial signaling molecule involved in systemic acquired resistance [36], was present at a significantly higher concentration in C3 (42.62 ng g^{-1}) than in C1 (31.54 ng g^{-1}). This pronounced increase suggests a direct contribution from the microbial consortium introduced through the biogas residue. In comparison, jasmonic acid (JA), which is generally associated with stress and damage responses [37], was detected at lower levels in C3, implying that the co-composting process imposed less stress and was therefore more favorable for compost quality.

In this study, C3 successfully preserved the fundamental growth-promoting compounds (e.g., IAA and GAs) derived from FW while simultaneously enriching cytokinins (e.g., DPU) and stress response hormones (e.g., SA) in the biogas residue. These combined effects enhanced the agricultural value of the final product, as reflected by the highest germination index observed in C3 (Figure 3b).

3.4. GHG Emission Profiles

GHG emission rates and cumulative emissions for the three composting groups are presented in Figure 4.

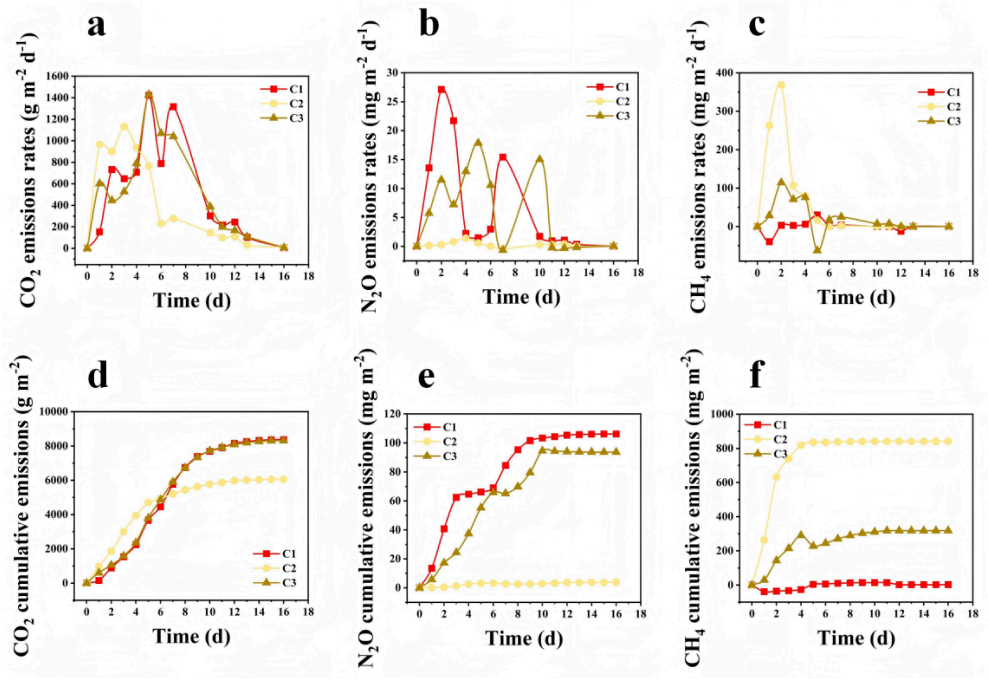

Figure 4. Variations in emission rates of (**a**) carbon dioxide (CO_2), (**b**) nitrous oxide (N_2O), and (**c**) methane (CH_4), and cumulative emissions of (**d**) CO_2, (**e**) N_2O and (**f**) CH_4 during composting.

3.4.1. CO_2 Emission Characteristics

In this study, changes in the CO_2 emission rates closely followed the temperature profiles observed across all three treatments (Figure 4a). This trend was consistent with previous findings showing that biochar-enhanced co-composting of chicken manure and FW produced comparable temperature dynamics and CO_2 emission patterns [38]. On the first day of composting, the CO_2 emission rates in C1, C2, and C3 were 6.41, 40.25, and 25.06 g m^{-1} h^{-1}, respectively, indicating that the biogas residue contained substantial amounts of readily mineralizable OM. For example, short-chain volatile fatty acids remaining after HSAD that were not fully converted to methane can strongly stimulate basal microbial respiration. This characteristic might partly explain the initiating effect of biogas residue on FW composting. In C2, the CO_2 emission rate declined rapidly after reaching a maximum on day 3, a pattern that closely matched its temperature profile. By the end of the composting period, C1 showed the highest cumulative CO_2 emissions, reflecting its high OM content (Figure 4d). However, cumulative CO_2 emissions in C3 also remained relatively high, reflecting efficient aerobic degradation during co-composting.

3.4.2. N_2O Emission Characteristics

In this study, the low porosity of the C1 compost pile on day 2 likely limited oxygen diffusion, thus inhibiting nitrification. Under these oxygen-deficient conditions, nitrate and nitrite were consumed by heterotrophic denitrifying microorganisms. At the same time, the low pH likely impeded complete denitrification, leading to N_2O accumulation and a peak emission rate of 27.12 mg m^{-2} d^{-1} [39]. During the subsequent thermophilic stage, elevated temperatures directly suppressed the activity of nitrifying bacteria, reducing the availability of substrates required for denitrification and, therefore, sharply decreasing N_2O emissions to 1.48 mg m^{-2} d^{-1} by day 5 [40]. Around day 7, intense microbial respiration under high temperature rapidly depleted oxygen within the pile (Figure 1a), leading to the formation of temporary anaerobic microsites [41]. The resulting localized anoxic conditions reactivated denitrifying microorganisms, triggering a secondary N_2O emission peak of 15.41 mg m^{-2} d^{-1}. Thereafter, as temperature continued to rise and readily available

substrates became depleted, the compost entered the maturation stage, during which N_2O emissions steadily declined from day 7 onward (Figure 4b).

Group C2 consistently demonstrated low N_2O emission rates, likely because the anaerobically digested substrate contained relatively low residual OM and rapidly entered a high-temperature phase at the early stage of composting. In C3, the N_2O emission peak occurred later (day 5) than in C1 (day 2). This delay was likely associated with the pH-buffering effect of the biogas residue amendment (Figure 1b), which alleviated the acidic conditions observed in C1 and promoted more complete denitrification, delaying the peak of N_2O release. The cumulative N_2O emissions in C1, C2, and C3 were 106.15, 3.83, and 93.72 mg m^{-2}, respectively (Figure 4e). These results indicated that biogas residue not only served as a composting initiator but also contributed to mitigating N_2O emissions during FW composting.

3.4.3. CH_4 Emission Characteristics

Significant CH_4 emissions were mainly observed in C2 and C3 (Figure 4c). In both groups, the maximum CH_4 emission flux occurred on day 2. It was significantly higher than the peak flux detected in C1 on day 5. This phenomenon might be attributed to methanogenic microorganisms introduced through the biogas residue, which remained active within localized anaerobic microenvironments in the compost piles and continuously generated methane from volatile fatty acids that were not completely degraded [42]. In comparison, CH_4 emission fluxes in C1 remained low throughout the composting process. During the maturation stage, CH_4 emissions in all three treatments declined to nearly zero, indicating that the compost piles had gradually stabilized. The cumulative CH_4 emissions followed the order C2 > C3 > C1, demonstrating that the addition of FW effectively alleviated the excessive CH_4 emissions associated with composting biogas residue alone (Figure 4f). Together with the cumulative N_2O emission results, these findings indicated that the co-composting strategy enabled synergistic mitigation of major GHGs, particularly CH_4 and N_2O.

3.5. Initiation Mechanism from the Perspective of Initial Physicochemical Characteristics of Materials

The initial characteristics of composting materials play a critical role in determining composting performance, particularly during the early and thermophilic stages [43]. Therefore, several key initial properties of the materials used in the three treatments were analyzed (Figure 5).

Analysis of the microbial communities based on 16S rRNA sequencing showed that microbial diversity in the initial composting materials followed the order C2 > C3 > C1 (Figures 5a and 6a). The addition of biogas residue in C3 directly introduced exogenous microorganisms into the system, shortening the microbial proliferation and adaptation period [44]. DHA is widely recognized as an indicator of overall microbial metabolic activity [45], while Biolog EcoPlates are commonly used to assess microbial metabolic capacity toward 31 representative carbon sources [19]. In this study, both DHA activity and microbial metabolic activity, expressed as AWCD, followed the order C1 > C3 > C2 (Figure 5b,c). These results suggested that the anaerobic microbial community present in C2 was not immediately adapted to aerobic composting conditions, which might have restricted microbial activity and reduced OM degradation efficiency.

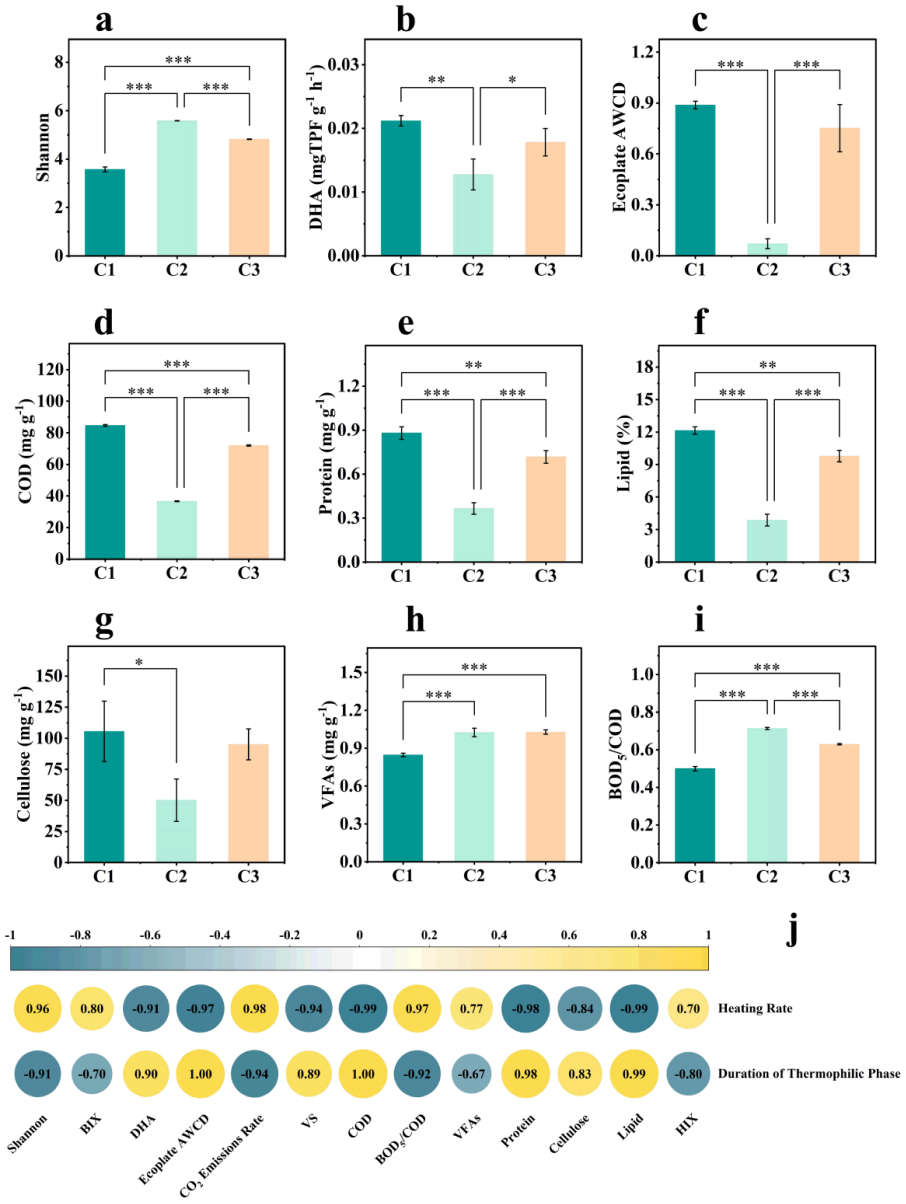

Figure 5. Characteristics of the initial composting materials (mean ± SD, n = 3): (**a**) Shannon index; (**b**) Dehydrogenase activity (DHA); (**c**) Ecoplate average well color development (AWCD); (**d**) Chemical oxygen demand (COD); (**e**) Protein; (**f**) Lipids; (**g**) Cellulose; (**h**) Volatile fatty acids; (**i**) BOD_5/COD; (**j**) Correlation analysis between the thermodynamic indicators and the initial material characteristics. Significance levels are represented by * ($p < 0.05$), ** ($p < 0.01$) and *** ($p < 0.001$).

To further elucidate the initiation mechanism of HSAD biogas residue, several initial substrate characteristics were evaluated, including: (1) COD, representing total OM content (Figure 5d); (2) recalcitrant organic compounds, such as proteins (Figure 5e), lipids (Figure 5f), and cellulose (Figure 5g); (3) readily biodegradable compounds, including short-chain volatile fatty acids (Figure 5h); and (4) the BOD_5/COD ratio, reflecting the biodegradability of organic compounds (Figure 5i). The results showed that C1 possessed not only the highest DHA activity but also the highest levels of COD (42.34 mg g^{-1}), OM (86.3%), protein (0.88 mg g^{-1}), lipid (12.14%), and cellulose (105.53 mg g^{-1}). Microorganisms can initially hydrolyze these complex organic compounds into monosaccharides and organic acids, which are subsequently utilized by thermophilic microorganisms during the thermophilic phase [19].

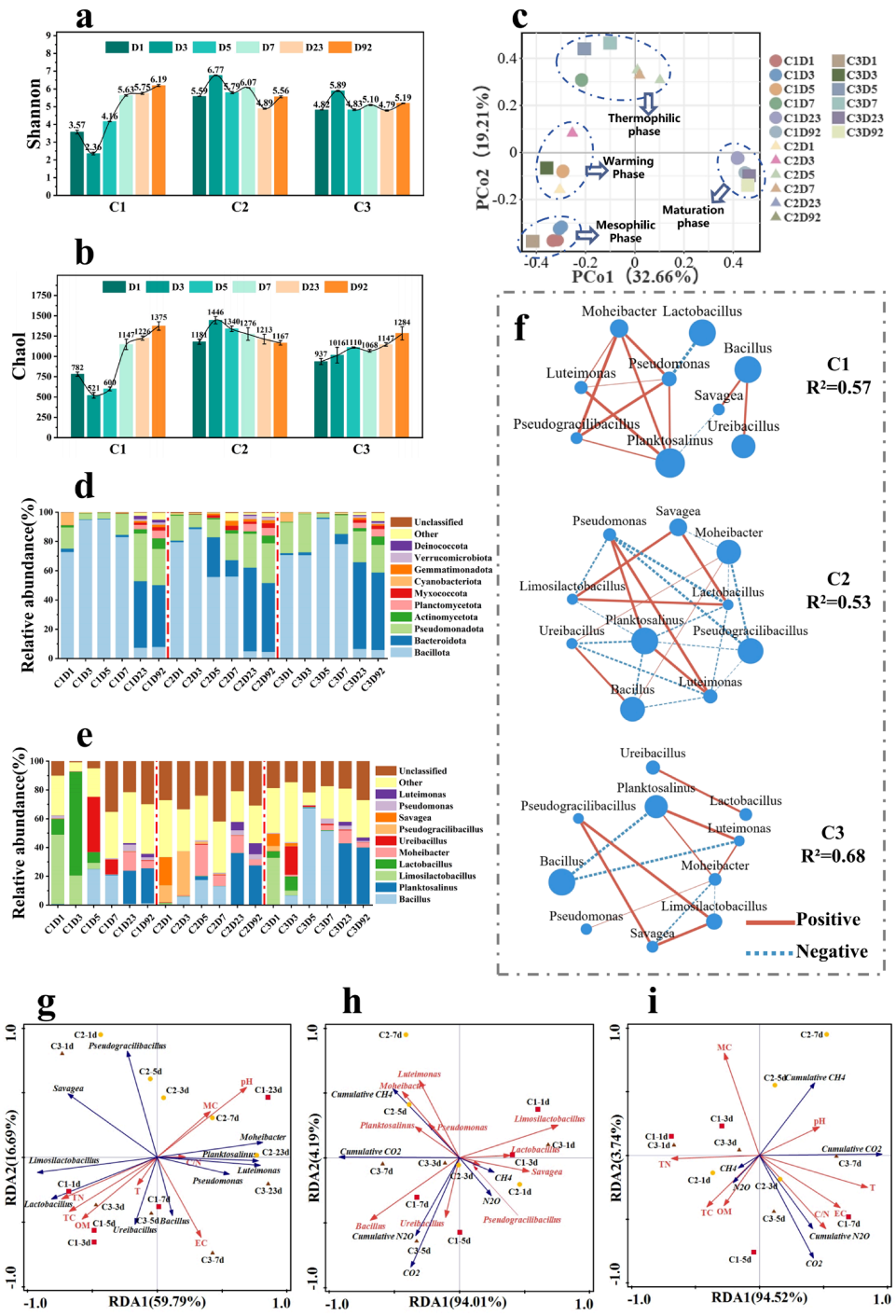

Figure 6. Microbial community structure across composting groups: Alpha diversity indices including (**a**) Shannon and (**b**) Chao l; Relative abundance of microbial communities at the phylum (**c**) and genus (**d**) levels; (**e**) Principal coordinates analysis (PCoA); (**f**) Species-level correlation network ($p < 0.05$) within each composting group; (**g**) Redundancy analysis (RDA) between environmental factors and the top 10 genera in relative abundance; (**h**) RDA between the top 10 microbial genera and greenhouse gas emission; (**i**) RDA between basic physicochemical properties and greenhouse gas emission.

C2 showed the highest volatile fatty acid concentration (2127.5 mg L^{-1}) and BOD_5/COD ratio (62.9%), indicating abundant readily degradable OM. These substrates were rapidly metabolized by microorganisms during the initial composting stage, generating substantial heat and leading to a rapid temperature increase. However, because C2 contained relatively low levels of recalcitrant substrates, including protein (0.37 mg g^{-1}),

lipid (3.87%), and cellulose (50.18 mg g^{-1}), there was insufficient continuous release of monosaccharides and organic acids. As a result, thermophilic microorganisms were unable to maintain prolonged heat production and led to the relatively short thermophilic phase.

In C3, the readily degradable substrates present in the biogas residue stimulated DHA activity, promoted electron transfer [45], and enhanced microbial energy conversion efficiency. This facilitated sequential degradation of the substrate throughout composting. Readily degradable compounds supported rapid temperature elevation, whereas more recalcitrant substrates sustained heat generation during the thermophilic phase. The synergistic interaction between these substrate fractions effectively overcame the limitations of both single-FW composting, which demonstrated slow heating, and sole biogas-residue composting, which showed an excessively short thermophilic period. Therefore, C3 showed both a rapid temperature increase (48% faster than in C1) and a prolonged thermophilic phase, with temperatures remaining above 55 °C for 10 days.

Correlation analysis was performed to identify the major initial factors influencing the thermodynamic behavior of the compost piles (Figure 5j). The results revealed strong positive correlations between the heating rate and both the Shannon index and the BOD_5/COD ratio. These results indicated that abundant microbial diversity and readily degradable OM are critical factors enabling rapid initiation of aerobic composting upon addition of biogas residue. In comparison, the duration of the thermophilic phase showed the strongest correlations with COD and microbial metabolic potential, suggesting that sustained high-temperature conditions depend primarily on adequate OM availability and strong microbial metabolic activity.

3.6. Microbial Community Analysis

3.6.1. Microbial Community Diversity

The Shannon index increased continuously from 3.57 on day 1 to 6.19 on day 92 in C1 (Figure 6a), indicating a substantial increase in microbial diversity throughout the composting process. In comparison, the Shannon index in C2 fluctuated significantly and gradually decreased as humification progressed. This decline was likely caused by limited carbon availability, which constrained microbial succession and community development [46]. In C3, the Shannon index increased steadily from 4.82 to 5.19, suggesting that co-composting promoted a more stable microbial community structure. The addition of biogas residue buffered the acidic conditions of FW, preventing a sharp reduction in microbial diversity and allowing the Shannon index to increase gradually before stabilizing. Similar trends were observed for the Chao1 index, which reflects microbial species richness (Figure 6b).

Principal coordinates analysis (PCoA) was performed to evaluate similarities in microbial community composition among the three treatments [47]. PC1 and PC2 explained 51.87% of the total variation in microbial communities. The composting process could be clearly divided into four stages: mesophilic, warming, thermophilic, and maturation (Figure 6c). In each treatment, microbial communities on day 1 (D1) differed significantly from those on day 92 (D92) ($p < 0.05$), demonstrating substantial shifts in community structure during composting. However, by D92, no significant differences were detected among three treatments ($p > 0.05$), indicating that the influence of the initial substrate composition had largely disappeared.

Significant differences among treatments were mainly observed during the early stages of composting (Figure 6c), particularly between C1 and C3 on days 3 ($p = 0.004$) and 23 ($p = 0.048$), and between C1 and C2 on days 3 ($p < 0.001$) and 7 ($p = 0.026$). These differences gradually diminished as composting progressed toward maturation. No significant differences were observed between C2 and C3 at any sampling point (all $p > 0.05$), indicating

highly similar microbial community composition and succession patterns in these two treatments. This suggested that the addition of FW did not substantially alter the microbial dynamics established by the biogas residue, further highlighting the important role of microorganisms introduced through biogas residue in initiating FW composting.

3.6.2. Microbial Community Composition

The phyla Bacillota and Bacteroidota revealed clear stage-dependent succession patterns, and their coordinated dynamics contributed substantially to the humification process (Figure 6d). On day 1, Bacillota was the dominant phylum across all treatments, and its abundance increased further after the thermophilic stage. This trend is likely related to the strong spore-forming ability and heat resistance of Bacillota members, which enabled continuous OM degradation under elevated temperatures [48]. During the thermophilic phase, Bacillota abundance remained highest in C3, suggesting that the biogas residue not only supplied readily degradable carbon to accelerate compost initiation but also provided heat-tolerant Bacillota, supporting prolonged microbial activity at high temperatures. In comparison, the abundance of Bacteroidota remained relatively low during the early stages but increased significantly during the maturation phase ($p < 0.001$), reaching the highest level in C3. Because this phylum includes important degraders of hemicellulose and proteins [28], its enrichment in C3 indicated enhanced humification during co-composting.

The initial microbial community in C1 was dominated by *Limosilactobacillus* and *Lactobacillus* (Figure 6e), which proliferated rapidly under low-pH (Figure 1b) and high-COD (Figure 5d) conditions through efficient glycolytic metabolism and acidification. In comparison, the alkaline conditions in C2 (Figure 1b) favored thermophilic and alkali-tolerant genera such as *Pseudogracilibacillus* and *Savagea* [49,50]. The microbial community in C3 demonstrated initial genera derived from those highly abundant in both C1 and C2.

During the thermophilic phase, thermophilic functional genera, including *Bacillus* [51] and *Ureibacillus* [52], became dominant in C1 and C3, promoting the degradation of recalcitrant OM. In comparison, the microbial community in C2 shifted from thermophilic bacteria toward the nitrogen-cycling genus *Moheibacter* [53]. The relative abundance of *Bacillus* in C3 reached 67.48%, which was significantly higher than that in other treatments. During the maturation stage, microbial communities in all treatments became dominated by *Moheibacter*, which metabolizes residual organic nitrogen, and *Planktosalinus*, a key genus associated with humification processes [54]. The significantly higher abundance of *Planktosalinus* in C3 (42.01%, $p < 0.001$) suggested that co-composting effectively promoted humification by improving carbon source diversity and enhancing environmental stability within the composting system.

3.6.3. Correlation Network Analysis

To further explore the potential role of internal microbial interactions during composting, co-occurrence networks were constructed at the genus level (Figure 6f). In C1, the thermophilic genera *Ureibacillus* and *Bacillus* displayed a strong positive correlation ($r = 0.790$, $p < 0.0001$). Together with *Savagea*, these microorganisms promoted close cooperative interactions with *Planktosalinus*, a core aerobic humification-related genus, as well as with the nitrogen-cycling genus *Moheibacter* ($r = 0.849$), the aerobic denitrifier *Pseudomonas* [55] ($r = 0.747$), and the starch-degrading genus *Luteimonas* [56] ($r = 0.925$). In C2, although *Bacillus* and *Ureibacillus* also showed strong positive interactions ($r = 0.881$, $p < 0.001$), the relatively short thermophilic phase resulted in pronounced antagonism between *Bacillus* and *Planktosalinus* ($r = -0.574$). The highly abundant *Pseudogracilibacillus* strongly inhibited *Pseudomonas* during the thermophilic stage ($r = -0.669$). The microbial network in C3 demonstrated a more cooperative interaction pattern. *Planktosalinus* and

Luteimonas showed an almost perfect positive correlation ($r = 0.997$, $p < 0.001$), and both genera interacted synergistically with *Moheibacter* ($r = 0.782$), promoting efficient humification during co-composting.

3.6.4. Redundancy Analysis

Redundancy analysis (RDA) was conducted to clarify the relationships among physicochemical properties, GHG emission, and microbial community succession during composting. The relationships between environmental variables and the top 10 dominant genera are presented in Figure 6g. RDA1 and RDA2 explained 59.79% and 16.69% of the total variance, respectively. TN (contribution = 37.3%, $p = 0.002$), temperature (T) (contribution = 17.8%, $p = 0.022$), and OM (contribution = 11.8%, $p = 0.042$) were identified as the major factors significantly affecting microbial community succession at the genus level. These environmental parameters were positively correlated with *Lactobacillus*, *Limosilactobacillus*, *Bacillus*, and *Ureibacillus*. In C1, the combination of high OM content and low pH during the initial stage favored the proliferation of *Limosilactobacillus* and *Lactobacillus*, whereas *Ureibacillus* and *Bacillus* became dominant by day 7. In comparison, the microbial communities in C2 and C3 during the early stage were primarily dominated by *Savagea* and *Pseudogracilibacillus*. By day 23, *Planktosalinus* and *Moheibacter* had become the dominant genera across all three treatments.

Figure 6h presents the RDA biplot using GHG emission fluxes and cumulative emissions as response variables and the top 10 microbial genera as explanatory variables. RDA1 and RDA2 accounted for 94.01% and 4.19% of the total variance, respectively. Among the dominant genera, only *Limosilactobacillus* ($p = 0.002$) and *Savagea* ($p = 0.022$) showed significant associations with GHG emission. *Limosilactobacillus* was negatively correlated with both CO_2 emission rate and cumulative CO_2 emissions, whereas *Savagea* demonstrated positive correlations with CH_4 and N_2O emission fluxes [49].

Figure 6i illustrates the RDA biplot with GHG emission fluxes and cumulative emissions as response variables and physicochemical parameters as explanatory variables. RDA1 and RDA2 explained 94.52% and 3.74% of the total variance, respectively. Among the measured physicochemical factors, only temperature significantly influenced GHG emission ($p = 0.002$). Temperature showed a positive correlation with CO_2 emission and weak negative correlations with CH_4 and N_2O emissions.

3.7. Metagenomic Analysis of the Nitrogen Metabolism

Given the significant differences among treatments in heating rate and duration of the thermophilic phase, their nitrogen transformation pathways and N_2O emission mechanisms might also vary. To further elucidate the differences in microbial functional genes associated with nitrogen metabolism, metagenomic sequencing was performed on compost samples collected on day 7 from each group (Figure 7). Although this single time point might not fully reflect the dynamics of functional genes throughout the composting process, day 7 was selected because it corresponded to the thermophilic phase for all three composting groups, which is widely recognized as the critical stage for nitrogen transformation, and because previous studies have demonstrated that denitrification dominates N_2O production during this phase [57], thus enabling the capture of the key functional genes responsible for differences in N_2O emission fluxes.

On day 7, C1 and C3 entered the thermophilic stage, and C2 had already progressed into the cooling stage. Metabolism, cellular processes, organismal systems, and environmental information processing were identified as the four major Level 1 Kyoto Encyclopedia of Genes and Genomes pathways associated with nitrogen metabolism across all treatments (Figure 7a). At Level 2, the dominant pathways included energy metabolism, global and

overview maps, amino acid metabolism, and carbohydrate metabolism. Volcano plot analysis revealed the following results (Figure 7b). In the C1 vs. C2 comparison, the numbers of downregulated and upregulated nitrogen metabolism-related genes were 470 and 413, respectively. In the C1 vs. C3 comparison, 316 genes were upregulated and 337 were downregulated. In the C2 vs. C3 comparison, 299 genes were upregulated and 406 were downregulated. Among these, the C1 vs. C2 comparison exhibited the highest total number of genes with significantly regulated abundance, indicating the greatest difference in nitrogen metabolism gene abundance profiles. This was primarily attributed to the fundamental differences in substrate origin and their associated microbial community structures.

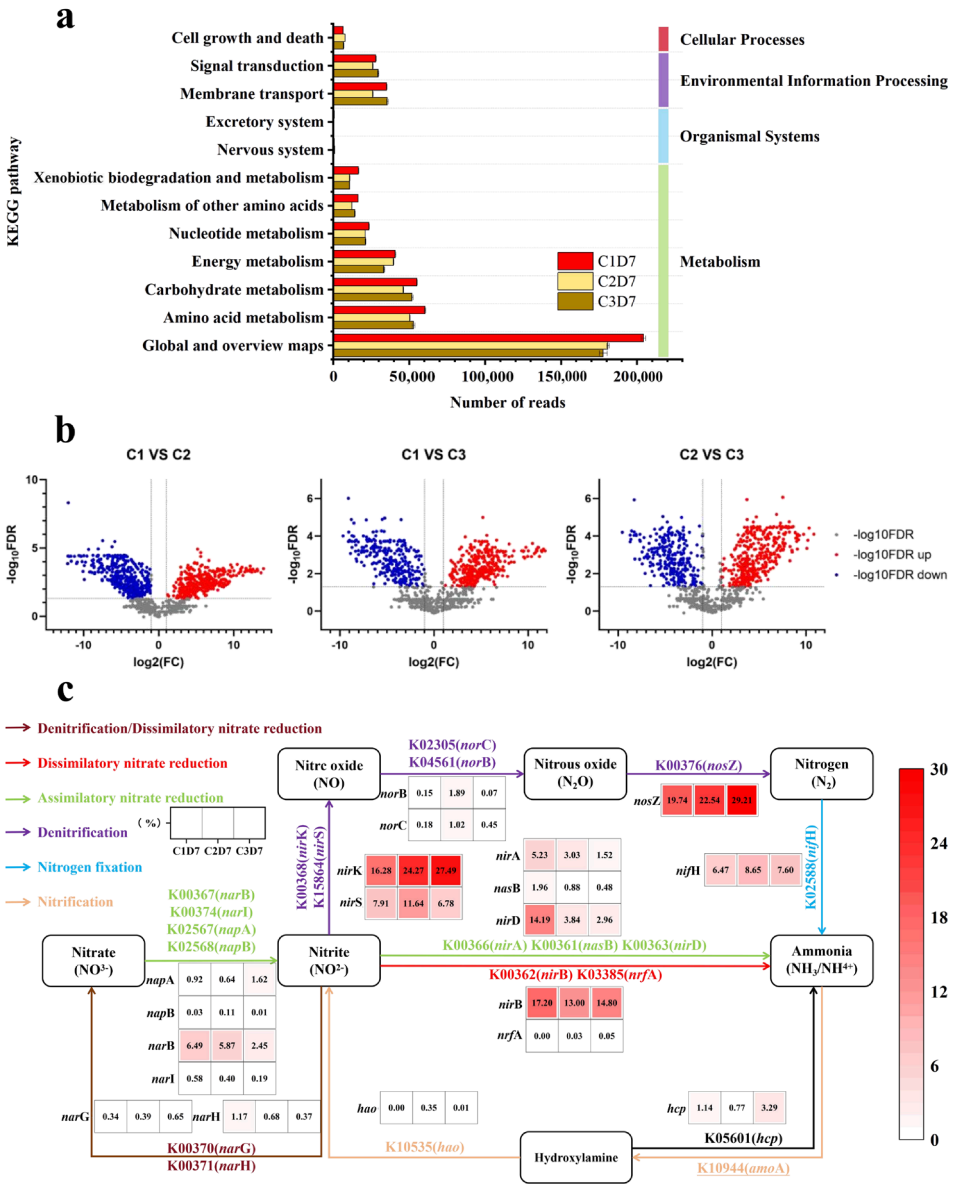

Figure 7. Metagenomic analysis of nitrogen metabolism: (**a**) Metagenomic data mapped to the primary and secondary pathways in Kyoto Encyclopedia of Genes and Genomes; (**b**) Volcano plot illustrating the differential abundance of nitrogen metabolism-related genes between groups, the grey line indicates the significance thresholds of $|\log_2(FC)| > 1$ and $-\log_{10}(FDR) > 1.3$; (**c**) Relative abundance of pathways and key functional genes.

On day 7, C1 (pH 7.11, 66.5 °C) showed the highest N_2O emission rate, while C2 (pH 9.14, 60.1 °C) and C3 (pH 8.38, 67.4 °C) both exhibited net N_2O consumption (–0.42 and –0.65 mg·m^{-2}·d^{-1}, respectively) (Figure 4b). The similar temperatures of C1 and C3

(p = 0.25) but opposite emission trends suggested that pH (All $p < 0.005$) was likely the key regulator controlling N_2O emissions. Consistently, previous studies have shown that the abundances of denitrification genes, including *nirS*, *nirK*, and *nosZ*, were positively correlated with pH [58]. Based on the functional gene abundances of nitrogen metabolism (Figure 7c), the terminal genes of the denitrification production pathway *norB*/*norC* were extremely low in C2 and C3 as well as in C1, making efficient N_2O production difficult. Therefore, the highest N_2O emission rate in C1 might be mainly associated with its lowest abundance of the N_2O reductase gene *nosZ*, corresponding to the lowest pH in C1, which severely limited the conversion of N_2O to N_2. In contrast, the *nosZ* gene abundances in C2 and C3 (22.54 and 29.21) were higher than that in C1 (19.74), corresponding to the higher pH in C2 and C3 than in C1, providing greater potential for N_2O reduction.

According to Liu et al. [59], high pH (e.g., 8.0) does not increase *nosZ* transcription but significantly promotes the post-translational assembly efficiency of *nosZ*, resulting in a higher abundance of functional *nosZ* enzyme. Thus, the high-pH environments of C2 and C3 likely led to greater *nosZ* activity, which together with the higher *nosZ* gene abundance allowed the rate of N_2O reduction to N_2 to exceed its production rate. Meanwhile, RDA (Figure 6i) showed a positive effect of temperature on N_2O emissions, yet net consumption still occurred in C3 at high temperature, further highlighting the regulatory role of pH. Thus, C3 harbored a denitrification functional gene profile (low *norB*/*norC*, high *nosZ*) under high-pH conditions, effectively shifting the N_2O balance toward net consumption.

3.8. PLS-PM Analysis

PLS-PM is a statistical tool for studying the effects of manifest variables on latent variables. In this study, it was applied to analyze how various parameters of the biogas residue-initiated aerobic composting process influenced the heating performance. The environmental factors (i.e., the physicochemical parameters during composting from Section 3.1), cumulative GHG emissions, and the relevant annotated data from reference databases (serving as manifest variables for chemoheterotrophic and thermotolerant microbial community, carbon metabolism and thermogenic functional genes; Tables S3 and S4) were used as manifest variables in PLS-PM, which systematically elucidated their causal relationships with compost heating performance (Figure 8).

Model results confirmed that environmental factors were the core drivers of the composting system (Figure 8a). They directly regulated carbon metabolism and thermogenic functional genes and cumulative GHG emissions. Although the direct effects of environmental factors on the chemoheterotrophic and thermotolerant microbial community were not significant, they exerted a powerful indirect influence via carbon metabolism and thermogenic functional genes, thereby shaping the final structure of the chemoheterotrophic and thermotolerant microbial community. In contrast, the chemoheterotrophic and thermotolerant microbial community showed a direct but marginally significant negative effect on cumulative GHG emissions. This suggests that dominant thermophilic microorganisms might inhibit methanogens and denitrifiers, partially offsetting GHG emission pressure. Therefore, in full-scale compost management systems, adjusting key parameters (such as C/N ratio, pH, and aeration conditions) is crucial to optimize chemoheterotrophic and thermotolerant microbial community while simultaneously reducing cumulative GHG emissions and improving energy efficiency.

A path analysis was conducted on all pathways influencing compost heating performance in the model (Figure 8b). Environmental factors exhibited a strong total negative effect on compost heating performance ($\lambda = -0.995$), which mainly stemmed from indirect pathways ($\lambda = -0.803$). This indicated that environmental factors do not directly inhibit heating. The total negative effect of the chemoheterotrophic and thermotolerant microbial

community suggested that under high temperatures, it caused energy consumption, which in turn hindered compost heating performance. Cumulative GHG emissions also had a significant direct negative effect on compost heating performance, which indicated that higher cumulative GHG emissions, particularly N_2O in C1 and CH_4 in C2, represented direct losses of energy substrates, thereby slowing heating rate and shortening the thermophilic phase, as evidenced by the balanced emission profile and superior heating performance of C3.

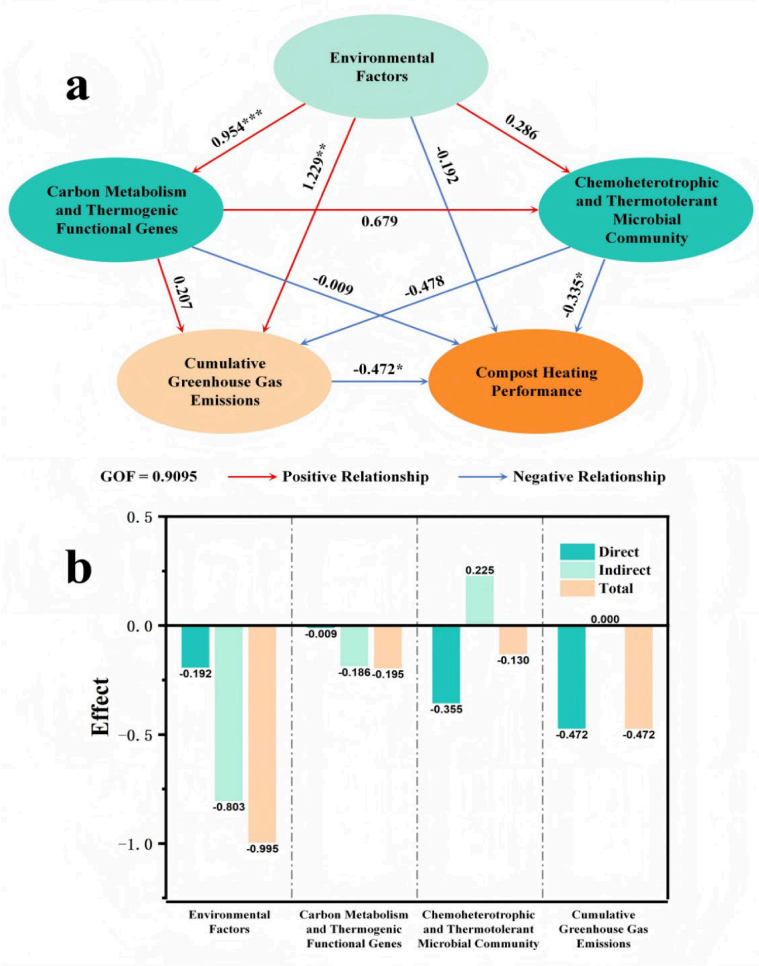

Figure 8. Partial Least Squares Path Modeling (PLS-PM) revealing the effect of environmental factors, carbon metabolism and thermogenic functional genes, chemoheterotrophic and thermotolerant microbial community, cumulative GHG emissions, and compost heating performance (**a**); Direct and indirect effect values from PLS-PM on compost heating performance (**b**). Significance levels are represented by * ($p < 0.05$), ** ($p < 0.01$) and *** ($p < 0.001$).

4. Conclusions

This study demonstrates that HSAD biogas residue can effectively initiate the aerobic composting of FW. In the treatment group using biogas residue as an initiator (C3), the compost pile reached its maximum temperature of 69.8 °C on day 5, 3 days earlier than in the FW-only treatment (C1), while maintaining a sufficiently long thermophilic phase of 10 days above 55 °C to ensure effective compost maturation. The final compost product from C3 showed the highest germination index of 220.65% and retained 24 types of phytohormones, preserving key growth-promoting and stress-resistance compounds. Analysis of the initial physicochemical properties of the composting materials indicated that the initiation mechanism of biogas residue was associated with the simultaneous introduction of exogenous microbial communities and readily degradable organic mat-

ter. These results demonstrate that using HSAD biogas residue as an initiator not only accelerates composting start-up but also extends the thermophilic phase and improves product quality. Moreover, C3 provided clear environmental advantages by achieving synergistic mitigation of both N_2O and CH_4 emissions during composting. During the thermophilic stage, Bacillota dominated the microbial community in C3, with a relative abundance of 95.52%, whereas Bacteroidota became enriched during the maturation stage, reaching 59.21%, promoting humification through an efficient microbial succession process. Metagenomic analysis further revealed that C3 exhibited net N_2O consumption on day 7 under high-pH conditions, consistent with its denitrification gene profile featuring low *norB*/*norC* and high *nosZ* abundances, indicating that under high pH the denitrification pathway was shifted toward N_2O reduction rather than production, thereby mitigating N_2O emissions even at elevated temperatures. PLS-PM revealed that environmental factors indirectly suppressed heating performance via carbon metabolism and thermogenic genes, while cumulative GHG emissions directly reduced heating efficiency. This study confirms that HSAD biogas residue is an effective initiator for FW aerobic composting. The work systematically clarifies the underlying initiation mechanisms, demonstrates the potential for reducing GHGs emission, and highlights the production of high-quality organic fertilizer with high nutrient content and a balanced phytohormone profile.

Supplementary Materials: The following supporting information can be downloaded at https://www.mdpi.com/article/10.3390/fermentation12070333/s1. Text S1–S5: Supplementary methods and analysis. Table S1: Heavy metal content of the compost products (mean ± standard error, n = 3); Table S2: Abbreviations and full names of phytohormones; Table S3: Composition of latent variables and their corresponding manifest variables in Partial Least Squares Path Modeling (PLS-PM), including Environmental Factors, Cumulative GHG Emissions, and Composting Heating Performance; Table S4: Latent variables (Chemoheterotrophic and Thermotolerant Microbial Community, Carbon Metabolism and Thermogenic Functional Genes) and their manifest variables with data in PLS-PM; Figure S1: Physicochemical properties of different treatment groups during composting: (a) moisture content; (b) EC; Figure S2: Three-dimensional excitation-emission matrix fluorescence spectra of different groups during the composting process: (a) C1; (b) C2; (c) C3.

Author Contributions: Conceptualization, S.Z. and A.L.; methodology, S.Z.; software, B.C.; validation, B.C., P.H. and H.Z.; formal analysis, B.C.; investigation, B.C., P.H. and H.Z.; resources, B.C.; data curation, B.C. and J.W.; writing—original draft preparation, B.C.; writing—review and editing, S.Z.; visualization, B.C.; supervision, S.Z.; project administration, S.Z.; funding acquisition, S.Z. All authors have read and agreed to the published version of the manuscript.

Funding: This research was supported by the Natural Science Foundation of China (52070177), the Natural Science Foundation of Xiamen (3502Z202673036) and the Guiding Project of Fujian Province of China (2026Y0031).

Institutional Review Board Statement: Not applicable.

Informed Consent Statement: Not applicable.

Data Availability Statement: Data are available upon request.

Conflicts of Interest: The authors declare no conflicts of interest.

References

1. Xu, Z.; Qi, C.; Zhang, L.; Ma, Y.; Li, J.; Li, G.; Luo, W. Bacterial dynamics and functions for gaseous emissions and humification in response to aeration intensities during kitchen waste composting. *Bioresour. Technol.* **2021**, *337*, 125369. [CrossRef] [PubMed]
2. Huang, W.; Shi, H.; Weng, Q.; Ding, S.; Lou, L. Disparities and mechanisms of carbon and nitrogen conversion during food waste composting with different bulking agents. *J. Environ. Manag.* **2024**, *351*, 119629. [CrossRef] [PubMed]

3. Mussa, S.; Farhan, M.; Ahmad, S.; Zahra, K.; Kanwal, A.; Khan, Q.F.; Afzaal, M.; Wahid, A.; Sarker, P.K.; El-Sheikh, M.A.; et al. Exploring the utility of different bulking agents for speeding up the composting process of household kitchen waste. *Sci. Rep.* **2025**, *15*, 2488. [CrossRef] [PubMed]
4. Mo, J.; Zhao, C.; Fang, C.; Long, Y.; Han, Y.; Mei, Q.; Wu, W. Pre-biodrying enhanced lignin degradation to promote aromatic macromolecular humic acid formation in double-phase composting. *Waste Manag.* **2025**, *202*, 114851. [CrossRef] [PubMed]
5. Li, Y.; Zhu, Z.; Li, S.; Tan, Y.; Xu, H.; Sheng, X.; Qi, B.; Wu, J.; Li, L.; Zhao, Z. Phase-specific microbial relay strategy enhances lipid degradation and humification in aerobic composting of lipid-rich food waste. *J. Environ. Manag.* **2025**, *390*, 126342. [CrossRef] [PubMed]
6. Wang, Z.; Hu, Y.; Wang, S.; Wu, G.; Zhan, X. A critical review on dry anaerobic digestion of organic waste: Characteristics, operational conditions, and improvement strategies. *Renew. Sustain. Energy Rev.* **2023**, *176*, 113208. [CrossRef]
7. Li, D.; Sun, M.; Xu, J.; Gong, T.; Ye, M.; Xiao, Y.; Yang, T. Effect of biochar derived from biogas residue on methane production during dry anaerobic fermentation of kitchen waste. *Waste Manag.* **2022**, *149*, 70–78. [CrossRef] [PubMed]
8. Pei, X.; Meng, Y.; Chen, C.; Li, Y.; Luo, Z.; Wang, P.; Liu, X.; Lin, X.; Zhang, Y.; Yang, S.; et al. Electrochemical oxidation of aquaculture wastewater by biogas residue biochar: Effects of chloride and removal of organic pollutants. *Biomass Bioenerg.* **2025**, *200*, 107959. [CrossRef]
9. Zhang, W.; Zhang, Y.; Zhao, M.; Wang, S.; Fan, X.; Zhou, N.; Fan, S. Preparation of mesoporous biogas residue biochar via a self-template strategy for efficient removal of ciprofloxacin: Effect of pyrolysis temperature. *J. Environ. Manag.* **2024**, *360*, 121140. [CrossRef] [PubMed]
10. Cao, B.; Li, M.; Zhang, T.; Gong, T.; Yang, T.; Xi, B.; Lu, H.; Wang, Z. Dynamics and mechanisms of atrazine adsorption on biogas-residue biochar with citric acid modification. *Sep. Purif. Technol.* **2024**, *337*, 126151. [CrossRef]
11. Rocamora, I.; Wagland, S.T.; Villa, R.; Simpson, E.W.; Fernández, O.; Bajón-Fernández, Y. Dry anaerobic digestion of organic waste: A review of operational parameters and their impact on process performance. *Bioresour. Technol.* **2020**, *299*, 122681. [CrossRef] [PubMed]
12. Bao, Y.; Fu, Y.; Wang, C.; Wang, H. An effective integrated system used in separating for anaerobic digestate and concentrating for biogas slurry. *Environ. Technol.* **2021**, *42*, 4434–4443. [CrossRef] [PubMed]
13. Zhao, Z.; Yan, L.; Li, G.; Rao, P.; Huo, B.; Li, T.; Li, Y.; Zhang, Z.; Sun, Y.; Xue, J. Food waste biogas residue-derived composite biochar for effective Cu^{2+} removal by capacitive deionization. *J. Environ. Chem. Eng.* **2025**, *13*, 117132. [CrossRef]
14. Achmon, Y.; Claypool, J.T.; Pace, S.; Simmons, B.A.; Singer, S.W.; Simmons, C.W. Assessment of biogas production and microbial ecology in a high solid anaerobic digestion of major California food processing residues. *Bioresour. Technol. Rep.* **2019**, *5*, 1–11. [CrossRef]
15. Huang, W.; Huang, W.; Yuan, T.; Zhao, Z.; Cai, W.; Zhang, Z.; Lei, Z.; Feng, C. Volatile fatty acids (VFAs) production from swine manure through short-term dry anaerobic digestion and its separation from nitrogen and phosphorus resources in the digestate. *Water Res.* **2016**, *90*, 344–353. [CrossRef] [PubMed]
16. Chen, Z.; Li, Y.; Peng, Y.; Ye, C.; Zhang, S. Effects of antibiotics on hydrolase activity and structure of microbial community during aerobic co-composting of food waste with sewage sludge. *Bioresour. Technol.* **2021**, *321*, 124506. [CrossRef] [PubMed]
17. Arab, G.; Razaviarani, V.; McCartney, D. Effects of digestate co-composting on curing phase of composting. *Bioresour. Technol. Rep.* **2022**, *19*, 101121. [CrossRef]
18. Hu, J.; Yang, Z.; Huang, Z.; Li, H.; Wu, Z.; Zhang, X.; Qin, X.; Li, C.; Ruan, M.; Zhou, K.; et al. Co-composting of sewage sludge and Phragmites australis using different insulating strategies. *Waste Manag.* **2020**, *108*, 1–12. [CrossRef] [PubMed]
19. Chen, Z.; Li, Y.; Peng, Y.; Mironov, V.; Chen, J.; Jin, H.; Zhang, S. Feasibility of sewage sludge and food waste aerobic co-composting: Physicochemical properties, microbial community structures, and contradiction between microbial metabolic activity and safety risks. *Sci. Total Environ.* **2022**, *825*, 154047. [CrossRef] [PubMed]
20. Chen, Z.; Zhang, S.; Li, Y.; Chi, B.; Huang, W.; Wu, J. Effects and mechanisms of kitchen waste organic fertilizers application on soil nitrogen transformation, plant pathogenic virulence genes, and metabolites. *Chem. Eng. J.* **2024**, *496*, 154125. [CrossRef]
21. Li, Y.; Zhang, S.; Chen, Z.; Huang, W.; Liu, Q.; Fang, H.; Chi, B.; Yang, N.; Zhang, Q. Deciphering the impact of organic loading rate and digestate recirculation on the occurrence patterns of antibiotics and antibiotic resistance genes in dry anaerobic digestion of kitchen waste. *Water Res.* **2024**, *261*, 122005. [CrossRef] [PubMed]
22. Chen, Z.; Zhang, S.; Li, Y.; Wang, Y. Characteristics of denitrification activity, functional genes, and denitrifying community composition in the composting process of kitchen and garden waste. *Bioresour. Technol.* **2023**, *381*, 129137. [CrossRef] [PubMed]
23. Gao, M.; Liang, F.; Yu, A.; Li, B.; Yang, L. Evaluation of stability and maturity during forced-aeration composting of chicken manure and sawdust at different C/N ratios. *Chemosphere* **2010**, *78*, 614–619. [CrossRef] [PubMed]
24. Diaz-Suntaxi, L.; Chicaiza Reisancho, E.R.; Valle, S.; Arias, P.E.; Aguiar-Novillo, S.; Ruíz Marmol, P.; Escobar-Machado, J.; Lopéz- Trabanco, P. Use of native microorganisms of the rhizophore of the amazon to accelerate the process of decomposition of organic agricultural residues. In *Proceedings of the MOL2NET'17, Conference on Molecular, Biomed., Comput. & Network Science and Engineering*, 3rd ed.; MDPI: Basel, Switzerland, 2017. [CrossRef]

25. Yang, Y.; Du, W.; Ren, X.; Cui, Z.; Zhou, W.; Lv, J. Effect of bean dregs amendment on the organic matter degradation, humification, maturity and stability of pig manure composting. *Sci. Total Environ.* **2020**, *708*, 134623. [CrossRef] [PubMed]
26. Azis, F.A.; Choo, M.; Suhaimi, H.; Abas, P.E. The Effect of Initial Carbon to Nitrogen Ratio on Kitchen Waste Composting Maturity. *Sustainability* **2023**, *15*, 6191. [CrossRef]
27. Chen, W.; Westerhoff, P.; Leenheer, J.A.; Booksh, K. Fluorescence Excitation−Emission Matrix Regional Integration to Quantify Spectra for Dissolved Organic Matter. *Environ. Sci. Technol.* **2003**, *37*, 5701–5710. [CrossRef] [PubMed]
28. Bai, B.; Wang, L.; Guan, F.; Pi, H.; Wang, A.; Zhai, L. Maturity phase is crucial for removing antibiotic resistance genes during composting: Novel insights into dissolved organic matter-microbial symbiosis system. *Bioresour. Technol.* **2025**, *431*, 132607. [CrossRef] [PubMed]
29. Huang, S.; Zheng, X.; Luo, L.; Ni, Y.; Yao, L.; Ni, W. Biostimulants in bioconversion compost of organic waste: A novel booster in sustainable agriculture. *J. Clean. Prod.* **2021**, *319*, 128704. [CrossRef]
30. Xing, C.-M.; Zhang, Y.-Y.; Zhang, Y.-F.; Meng, Y.-F.; Wu, Q.-L.; Yan, B.; Wu, Y.-H.; Wang, H.-Z.; Du, J.-S.; Guo, W.-Q. Municipal sludge as precursors in Chinese medicinal herbal residues composting for plant-growth biostimulant production: Priming effects and microbial mechanism. *Resour. Conserv. Recycl.* **2025**, *217*, 108221. [CrossRef]
31. Fan, Y.; Yu, K.; Zheng, H.; Chen, Y.; Zhao, R.; Li, Y.; Zheng, Z. A high-yielding strain of indole-3-acetic acid isolated from food waste compost: Metabolic pathways, optimization of fermentation conditions, and application. *Environ. Technol.* **2023**, *44*, 4199–4209. [CrossRef] [PubMed]
32. Kumari, S.; Prabha, C.; Singh, A.; Kumari, S.; Kiran, S. Optimization of Indole-3-Acetic Acid Production by Diazotrophic B. subtilis DR2 (KP455653), Isolated from Rhizosphere of Eragrostis cynosuroides. *Int. J. Pharma Med. Biol. Sci.* **2018**, *7*, 20–27. [CrossRef]
33. Strader, L.C.; Culler, A.H.; Cohen, J.D.; Bartel, B. Conversion of Endogenous Indole-3-Butyric Acid to Indole-3-Acetic Acid Drives Cell Expansion in Arabidopsis Seedlings. *Plant Physiol.* **2010**, *153*, 1577–1586. [CrossRef] [PubMed]
34. Ogawa, M.; Hanada, A.; Yamauchi, Y.; Kuwahara, A.; Kamiya, Y.; Yamaguchi, S. Gibberellin Biosynthesis and Response during Arabidopsis Seed Germination. *Plant Cell* **2003**, *15*, 1591–1604. [CrossRef] [PubMed]
35. Antoniadi, I.; Mateo-Bonmatí, E.; Pernisová, M.; Brunoni, F.; Antoniadi, M.; Villalonga, M.G.-A.; Ament, A.; Karády, M.; Turnbull, C.; Doležal, K.; et al. IPT9, a cis-zeatin cytokinin biosynthesis gene, promotes root growth. *Front. Plant Sci.* **2022**, *13*, 932008. [CrossRef] [PubMed]
36. Gaffney, T.; Friedrich, L.; Vernooij, B.; Negrotto, D.; Nye, G.; Uknes, S.; Ward, E.; Kessmann, H.; Ryals, J. Requirement of Salicylic Acid for the Induction of Systemic Acquired Resistance. *Science* **1993**, *261*, 754–756. [CrossRef] [PubMed]
37. Levak, V.; Povalej, T.M.; Pogačar, K.; Stare, K.; Zagorščak, M.; Hawkins, T.; Robson, J.; Dobnik, D.; Lukan, T.; Gruden, K. Jasmonic acid and salicylic acid interact to determine spatial regulation of gene expression responses in potato leaf to herbivory by Colorado potato beetle and mechanical wounding. *Plant Cell Physiol.* **2025**, *66*, 1878–1890. [CrossRef] [PubMed]
38. Chen, H.; Awasthi, S.K.; Liu, T.; Duan, Y.; Ren, X.; Zhang, Z.; Pandey, A.; Awasthi, M.K. Effects of microbial culture and chicken manure biochar on compost maturity and greenhouse gas emissions during chicken manure composting. *J. Hazard. Mater.* **2020**, *389*, 121908. [CrossRef] [PubMed]
39. Wu, X.; Zhao, X.; Yi, G.; Zhang, W.; Gao, R.; Tang, D.K.H.; Xiao, R.; Zhang, Z.; Yao, Y.; Li, R. Promoting nitrogen conversion in aerobic biotransformation of swine slurry with the co-application of manganese sulfate and biochar. *J. Environ. Manag.* **2024**, *356*, 120604. [CrossRef] [PubMed]
40. Ma, X.; Bai, H.; Li, G.; Li, L.; Meng, H.; Liu, Y.; Yuan, J. Effects of nitrification inhibitors DCD and DMPP on maturity, N2O and NH3 emissions during manure composting. *J. Environ. Manag.* **2025**, *380*, 124895. [CrossRef] [PubMed]
41. Song, J.; Paul, F.; Terry, B. *Bioremediation of Petroleum Hydrocarbons in Heterogeneous Soils*; Western Research Institute (WRI): Pittsburgh, PA, USA; Morgantown, WV, USA, 2006. [CrossRef] [PubMed]
42. Ge, J.; Huang, G.; Yang, Z.; Huang, J.; Han, L. Characterization of the Dynamic Thickness of the Aerobic Layer during Pig Manure Aerobic Composting by Fourier Transform Infrared Microspectroscopy. *Environ. Sci. Technol.* **2014**, *48*, 5043–5050. [CrossRef] [PubMed]
43. Liu, X.; Zubair, M.; Kong, L.; Shi, Y.; Zhou, H.; Tong, L.; Zhu, R.; Lv, Y.; Li, Z. Shifts in bacterial diversity characteristics during the primary and secondary fermentation stages of bio-compost inoculated with effective microorganisms agent. *Bioresour. Technol.* **2023**, *382*, 129163. [CrossRef] [PubMed]
44. Zhang, C.; de Pasquale, S.; Hartman, K.; Stanley, C.E.; Berendsen, R.L.; van der Heijden, M.G.A. The microbial contribution to litter decomposition and plant growth. *Environ. Microbiol. Rep.* **2024**, *16*, e13205. [CrossRef] [PubMed]
45. Barrena, R.; Vazquez, F.; Sanchez, A. Dehydrogenase activity as a method for monitoring the composting process. *Bioresour. Technol.* **2008**, *99*, 905–908. [CrossRef] [PubMed]
46. Chen, P.; Zhang, L.; Li, Y.; Liang, J. Insight to maturity during biogas residue from food waste composting in terms of multivariable interaction. *Environ. Sci. Pollut. Res.* **2022**, *29*, 71785–71795. [CrossRef] [PubMed]

47. Zhang, Y.; Yang, B.; Peng, S.; Zhang, Z.; Cai, S.; Yu, J.; Wang, D.; Zhang, W. Mechanistic insights into chemical conditioning on transformation of dissolved organic matter and plant biostimulants production during sludge aerobic composting. *Water Res.* **2024**, *255*, 121446. [CrossRef] [PubMed]
48. Han, W.; Chen, S.; Tan, X.; Li, X.; Pan, H.; Ma, P.; Wu, Z.; Xie, Q. Microbial community succession in response to sludge composting efficiency and heavy metal detoxification during municipal sludge composting. *Front. Microbiol.* **2022**, *13*, 1015949. [CrossRef] [PubMed]
49. Liu, S.; Yang, X.; Yao, X. Effects of pH on the biodegradation characteristics of thermophilic micro-aerobic digestion for sludge stabilization. *RSC Adv.* **2019**, *9*, 8379–8388. [CrossRef] [PubMed]
50. Fu, X.; Zuo, H.; Wang, Z.; Shang, P.; Li, Z.; Li, J.; Zhan, Y.; Wang, Q.; Arslan, M.; Gamal El-Din, M.; et al. Extreme thermophilic microbial inoculation for reducing NH_3 and N_2O emissions in hyperthermophilic aerobic composting of refinery waste activated sludge. *J. Environ. Manag.* **2025**, *380*, 124870. [CrossRef] [PubMed]
51. Zainudin, M.H.M.; Singam, J.T.; Sazili, A.Q.; Shirai, Y.; Hassan, M.A. Indigenous cellulolytic aerobic and facultative anaerobic bacterial community enhanced the composting of rice straw and chicken manure with biochar addition. *Sci. Rep.* **2022**, *12*, 5930. [CrossRef] [PubMed]
52. Santana, M.M.; Gonzalez, J.M. High temperature microbial activity in upper soil layers. *FEMS Microbiol. Lett.* **2015**, *362*, fnv182. [CrossRef] [PubMed]
53. Liu, X.; Gao, L.; Yu, C.; Jin, W.; Xu, X.; Liu, S.; Yang, F. Nitrogen losses at varying heights in full-scale functional membrane-covered aerobic composting: Insights into interactions between microbial communities and environmental factors. *J. Environ. Chem. Eng.* **2025**, *13*, 117468. [CrossRef]
54. Song, Y.; Li, R.; Wang, Y.; Hou, Y.; Chen, G.; Yan, B.; Cheng, Z.; Mu, L. Co-composting of cattle manure and wheat straw covered with a semipermeable membrane: Organic matter humification and bacterial community succession. *Environ. Sci. Pollut. Res.* **2022**, *30*, 32776–32789. [CrossRef] [PubMed]
55. Banu, J.R.; Sugitha, S.; Kavitha, S.; Kannah, R.Y.; Merrylin, J.; Kumar, G. Lignocellulosic Biomass Pretreatment for Enhanced Bioenergy Recovery: Effect of Lignocelluloses Recalcitrance and Enhancement Strategies. *Front. Energy Res.* **2021**, *9*, 646057. [CrossRef]
56. Yuan, N.; Wang, K.; Zhou, J.; Luo, N.; Yu, R. Biochar-supported Fe_3O_4 nanoparticles affects bacterial community diversity and phosphorus speciation transformation during pig manure aerobic composting by generating hydroxyl radicals and hydrogen peroxide. *J. Environ. Chem. Eng.* **2025**, *13*, 115364. [CrossRef]
57. Chen, Z.; Zhang, S.; Li, Y.; Guo, Z. Investigating nitrous oxide emissions and mechanisms in kitchen waste composting with leachate reuse. *Chem. Eng. J.* **2023**, *476*, 146813. [CrossRef]
58. Huang, W.; Bao, R.; Peng, Y.; Li, Q. Regulation of manganese dioxide on sludge composting to inhibit nitrous oxide generation and promote nitrogen fixation. *Chem. Eng. J.* **2025**, *519*, 165150. [CrossRef]
59. Liu, B.; Mørkved, P.T.; Frostegård, Å.; Bakken, L.R. Denitrification gene pools, transcription and kinetics of NO, N_2O and N_2 production as affected by soil pH. *FEMS Microbiol. Ecol.* **2010**, *72*, 407–417. [CrossRef] [PubMed]